$L_{2,3}$ edges of tetrahedrally coordinated d^0 transition-metal oxyanions XO_4^{n-}

1993 J. Phys.: Condens. Matter 5 9379

(http://iopscience.iop.org/0953-8984/5/50/018)

J. Phys.: Condens. Matter 5 (1993) 9379–9392. Printed in the UK

$L_{2,3}$ edges of tetrahedrally coordinated d^0 transition-metal oxyanions XO_4^{n-}

R Brydson†, L A J Garvie‡, A J Craven‡, H Sauer§, F Hofer‖ and G Cressey¶

† Department of Materials Science and Engineering, University of Surrey, Guildford, Surrey GU2 5XH, UK

‡ Department of Physics and Astronomy, University of Glasgow, Glasgow G12 8QQ, UK

§ Fritz-Haber-Institut der Max-Planck-Gesellschaft, Faradayweg 4-6, D14195 Berlin 33, Federal Republic of Germany

‖ Forschungsinstitut fur Elektronenmikroskopie und Feinstrukturforschung, Technische Universitat Graz, Steyrergasse 17, A-8010 Graz, Austria

¶ Department of Mineralogy, The Natural History Museum, Cromwell Road, London SW7 5BD, UK

Received 21 September 1993

Abstract. The $L_{2,3}$ edges of compounds containing tetrahedrally coordinated, isoelectronic d^0 transition-metal oxyanions, TiO_4^{4-}, VO_4^{3-}, CrO_4^{2-} and MnO_4^- have been measured using electron energy-loss spectroscopy (EELS). The general shape of the electron energy-loss near-edge fine structure (ELNES) is found to be remarkably similar for these oxyanions and arises from the atomic multiplet spectrum of the d^0 transition-metal ion modified by the tetrahedral field due to the oxygen ligands. The observed structure is also discussed within the framework of molecular-orbital (MO) theory. The possibilities of using these spectra as fingerprints for d^0 transition-metal ions in tetrahedral coordination is discussed. The structure observed at the O K edges is also commented upon in the light of these findings.

1. Introduction

The $L_{2,3}$ edges of 3d and 4d transition metals, as well as the $M_{4,5}$ edges of the rare earths, exhibit strong, sharp features in the electron energy-loss spectroscopy (EELS) spectrum known as white lines (since they were originally recorded as lines on a photographic plate). The presence of these features make detection of these elements in a complex microstructure relatively straightforward. In recent years it has also become apparent that analysis of the intensity distribution and energy onset of the energy-loss near-edge structure (ELNES) can allow determination of the valency of the atom undergoing excitation [1, 2].

In the case of the 3d transition-metal oxides and related compounds, the major features of the $L_{2,3}$ edges arise from the dipole-allowed excitation of electrons in the inner 2p shell of the transition-metal atom to the relatively narrow unoccupied 3d band, which is of predominantly metal 3d character hybridized with a significant amount of O 2p character. Two white-line components are observed, which correspond to the two ways in which the spin quantum number s can couple to the orbital angular-momentum quantum number l to give the total angular-momentum quantum number $j = l \pm s$ of the 2p core-hole state created upon excitation. Thus for the $L_{2,3}$ edges, the two components observed arise from transitions from the $2p_{3/2}$ (L_3 edge) and $2p_{1/2}$ levels (L_2 edge). These two features are separated by the spin–orbit splitting of the inner 2p shell, with the L_2 edge sitting on the

0953-8984/93/509379+14$07.50

high-energy background of the L_3 edge. The intrinsic width of the L_2 edge is considerably broader than that of the L_3 owing to the existence of an extra Coster–Kronig Auger decay channel in which the $2p_{1/2}$ core-hole state decays via production of a $2p_{3/2}$ core hole and the simultaneous ejection of a d electron. This results in a shorter final-state lifetime of the $2p_{1/2}$ core-hole state, which causes a relative broadening in energy by the uncertainty principle. Assuming that all other effects are equal, consideration of the degeneracy of the initial states (equal to $2j + 1$) leads to the conclusion that the L_3 white line should be twice as intense as the L_2 white line. However, experimentally the L_3/L_2 white-line intensity ratio has been shown to deviate considerably from the statistical ratio of 2:1 that would be expected if the excited electron were probing the extended band structure. This anomalous behaviour was subsequently shown to arise from the fact that these spectra reflect quasiatomic transitions from the $2p^63d^n$ initial state to the $2p^53d^{n+1}$ final state of the transition-metal ion, with only a relatively minor modification due to its solid-state environment [3, 4]. This is predominantly due to the narrow width of the metal 3d band combined with the effect of the 2p core-hole potential which causes the local d-like unoccupied density of states (DOS) probed by the excited electron to decouple from the extended band structure and hence retain much of its atomic character. In other words the white lines arise from transitions to atomic-like bound states.

In the $2p^63d^n$ initial state, interactions between 3d electrons can cause a number of different possible ground states (an initial-state multiplet). In the case of the $2p^63d^0$ initial state we only have a single ground state (^1S). In the $2p^53d^1$ final state, the 2p core-hole spin–orbit coupling (which splits the edge into the L_3 and L_2 components) together with the various interactions between the core hole and the distribution of electrons in the final state leads to a multiplicity of possible dipole-allowed final states (a final-state multiplet). The energies and intensities of the observed transitions in this *atomic multiplet spectrum* correspond to the energy differences and degree of orbital overlap between the ground state and all final states in the final-state multiplet. The influence of the crystal field due to the ligands will break the spherical symmetry around the atom and affect the accessible final states, shifting them in energy and changing their degree of overlap with the ground state. The symmetry of the crystal field essentially mixes in new final states, which were forbidden in spherical symmetry, while the magnitude of the crystal field affects the relative intensities and energy positions of the various transitions observed.

In the dipole limit of small momentum transfer, ELNES measurements correspond directly to x-ray absorption near-edge structure (XANES) data. De Groot *et al* [5, 6] have measured and modelled the $L_{2,3}$ edges of a range of 3d transition-metal compounds containing transition-metal ions in octahedral O_h symmetry using x-ray absorption spectroscopy (XAS). Theoretical modelling using atomic multiplet theory revealed that, for the case of d^0 transition-metal ions, both the L_3 and L_2 white lines split into two main components, which can be identified with the low-energy t_{2g}^* and higher-energy e_g^* antibonding molecular orbitals (MOs) (the asterisk denotes that the orbital is antibonding in character). These are formed by both σ- and π-type interactions of the atomic orbitals of the octahedrally coordinated transition-metal ion with those on the ligand atoms [7]. However, the observed energy splitting between these components is, in general, not equal to the magnitude of the crystal field (commonly referred to as $10Dq$) owing to the competition of the various quasiatomic effects. As a general point, the crystal-field splitting is expected to be more faithfully reproduced at the ligand core-loss edge where the core-hole interactions are generally less and the excited electron is more directly probing the extended band structure of the material [8]. For the case of d^n ions (i.e. those containing d electrons in the ground state) the situation is more complicated, owing to the large number of possible final and initial states

in the atomic multiplet spectrum, and it becomes much more difficult to directly identify the t_{2g}^* and e_g^* crystal-field components in the metal $L_{2,3}$ spectra [6]. Distortions from perfect O_h symmetry generally result in a broadening and in some cases splitting of features, as is observed for the series $SrTiO_3$, TiO_2 rutile and TiO_2 anatase (O_h, D_{2h} and D_{2d} symmetry at the Ti^{4+} site respectively) [2]. More recently van der Laan and Kirkman [9] have published improved atomic multiplet calculations for 3d transition-metal ions in both octahedral and tetrahedral symmetry.

We have investigated the $L_{2,3}$ ELNES of a number of materials containing d^0 transition-metal ions in tetrahedral T_d symmetry. This work constitutes a logical extension of previous studies [5, 6, 10] and hopefully provides an insight into whether it is possible to extract coordination symmetries as well as valence states from quasiatomic spectra measured from complex systems.

2. Experiment

The compounds chosen were potassium permanganate, $KMnO_4$, crocoite, $PbCrO_4$ and vanadinite, $Pb_5(VO_4)_3Cl$. The former was a pure laboratory reagent, while the latter two were single-crystal mineralogical specimens. Orthorhombic barium orthotitanate, Ba_2TiO_4, was prepared as in [11]. All of the samples were prepared for EELS analysis by crushing selected crystals in acetone and pipetting the suspension onto 'holey' carbon films. $KMnO_4$ was observed to recrystallize on the support film. EELS data were recorded from thin areas over holes in the support film.

The majority of EELS data were acquired on a VG HB5 scanning transmission electron microscope (STEM) operated at 100 keV and equipped with a field emission gun and Gatan 666 parallel EELS spectrometer and recording system. The emission current drawn from the field emission tip was 5 μA, which resulted in an energy resolution at the zero loss peak of $\sim$ 0.35 eV. The convergence and collection semi-angles were 11 and 12.5 mrad respectively. The absolute energies of ELNES features and the dispersion of the spectrometer system were determined by application of known voltages to the spectrometer drift tube. An energy dispersion of 0.1 eV was employed allowing the ELNES to be clearly discerned. The majority of spectra were collected with an integration time of 8 s by rastering an area of typically 60 nm by 50 nm. Owing to the extreme electron-beam sensitivity of $KMnO_4$, spectra for this material were recorded with a 2 s acquisition time, a highly defocused probe and low beam current together with the simultaneous movement of the sample area to undamaged regions. Failure to observe this procedure resulted in an Mn $L_{2,3}$ spectrum that resembled that obtained from compounds containing Mn^{4+} in more or less octahedral coordination [12] (presumably $KMnO_4$ transforms to MnO_2 under the electron beam with the removal of K and O). Experimental data were corrected for dark current and the background subtracted. The effects of specimen thickness were removed via a Fourier-ratio deconvolution procedure [13]. The spectra of Ba_2TiO_4 were measured at a comparable energy resolution on a different field emission STEM equipped with a parallel recording system, which has been described elsewhere [14]; spectra were obtained from thin areas and deconvolution was deemed unnecessary for the comparison of near-edge features. The Mn $L_{2,3}$ x-ray absorption data for $KMnO_4$ (powdered with graphite) were recorded on beamline 5U.1 of the Daresbury Synchrotron Radiation Source using electron-yield detection methods [15].

3. Results

The background-subtracted $L_{2,3}$ edges of the tetrahedrally coordinated oxyanions MnO_4^-, CrO_4^{2-}, VO_4^{3-} and TiO_4^{4-} are shown in figure 1, curves a–d respectively. The spectrum of MnO_4^- is of relatively poor statistical quality for the reasons mentioned above. Consequently in figure 2 we show the Mn $L_{2,3}$ XANES of $KMnO_4$ measured with a resolution of 0.3 eV for comparative purposes [15]. The corresponding O K edges for MnO_4^-, CrO_4^{2-} and VO_4^{3-} are shown in figure 3, curves a–c respectively. The beam sensitivity of $KMnO_4$ causes us to regard the spectrum in figure 3 (curve a) with caution. Considerable changes were noted in the O K edge of $KMnO_4$ with increasing dose; however, we believe that the spectrum in figure 3 (curve a) is representative of the minimally damaged material. Further work is required in order to resolve this point. All spectra are shown on a relative energy scale. For completeness, tables 1 and 2 list the energies and approximate relative intensities of the various features labelled in figures 1–3. We stress that the data for MnO_4^- are incomplete; however we have included it in the following discussion of the general trends observed in the oxyanion spectra.

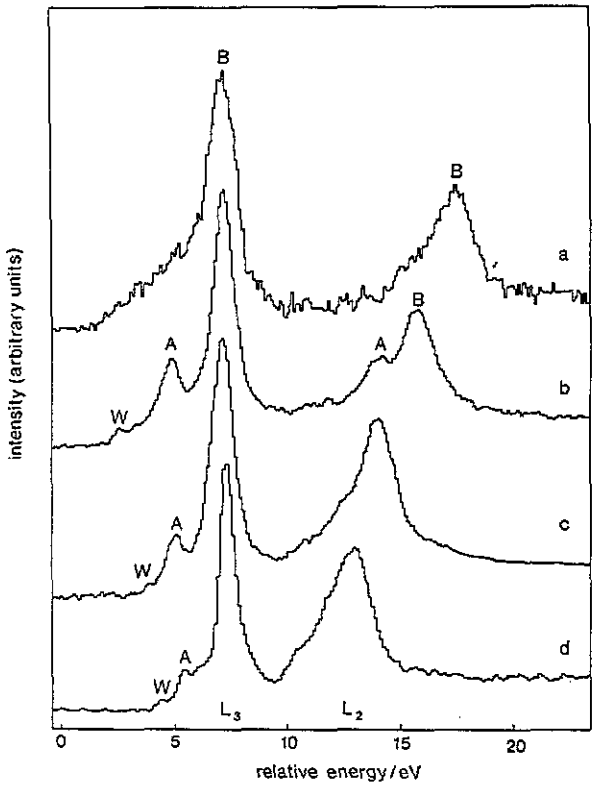

Figure 1. a, Mn $L_{2,3}$ ELNES of $KMnO_4$; b, Cr $L_{2,3}$ ELNES of $PbCrO_4$; c, V $L_{2,3}$ ELNES of $Pb_5(VO_4)_3Cl$; d, Ti $L_{2,3}$ ELNES of orthorhombic Ba_2TiO_4. The spectra are shown on a relative energy scale and have been aligned at peak B.

It is immediately apparent that the spin–orbit splittings between the L_3 and L_2 edges decrease in the order Mn(VII) > Cr(VI) > V(V) > Ti(IV), where the roman numeral

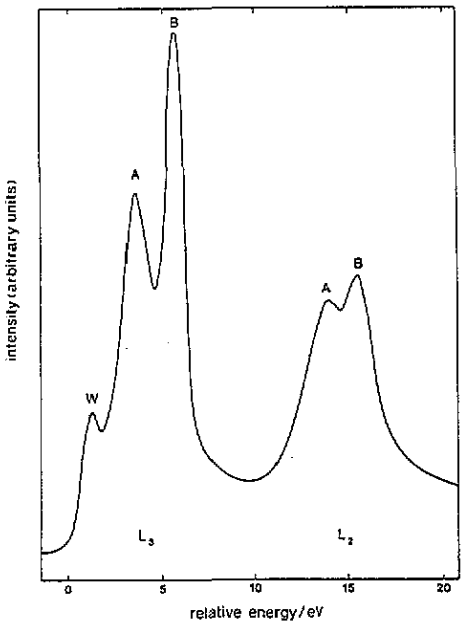

Figure 2. Mn $L_{2,3}$ XANES of $KMnO_4$ for comparison with figure 1, curve a.

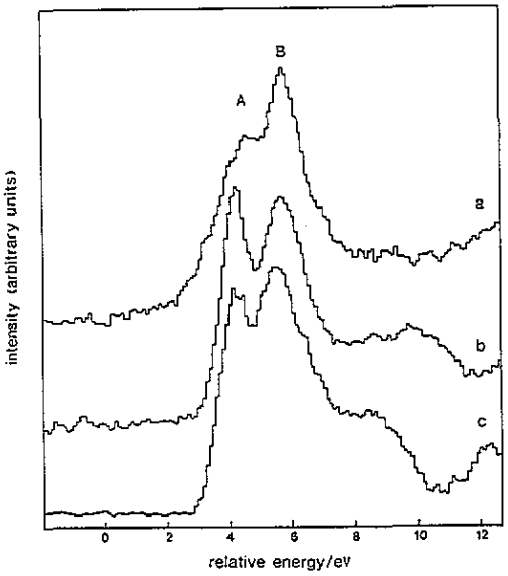

Figure 3. O K ELNES of: a, $KmNO_4$—this is assumed to be undamaged (see text); b, $PbCrO_4$; and c, $Pb_5(VO_4)_3Cl$. The spectra are shown on a relative energy scale and have been aligned at peak B.

Table 1. Absolute energies (and intensity ratios) of the various features at the transition-metal $L_{2,3}$ edges of the oxyanions shown in figures 1 and 2. Values have only been given where an accurate determination was possible. The values in brackets for $KMnO_4$ were obtained from the XANES data. The absolute energy values are accurate to $\sim \pm 0.5$ eV. Approximate intensity ratios were determined by a Gaussian fitting procedure.

	Peak position (eV) L_3 edge			Intensity ratio	Peak position (eV) L_2 edge	
Oxyanion	W	A	B	I_A/I_B	A	B
MnO_4^-	(641.3)	(643.5)	645.6	(0.7)	(654.3)	656.0
CrO_4^{2-}	576.3	578.6	580.9	0.3	587.8	589.5
VO_4^{3-}	515.0	516.2	518.2	0.1	523.6	525.1
TiO_4^{4-}	456.4	457.4	459.3	0.1	—	465.2

in brackets denotes the formal oxidation state of the d^0 transition-metal ion. However, inspection of the spectra in figures 1 and 2 reveals that the general form of the ELNESs are remarkably similar, taking into account the poor statistics of figure 1, curve a. Both the L_3 and L_2 edges show a splitting of the white line into two components, the lower-energy component A being of considerably lower relative intensity than the higher-energy component B. In the case of MnO_4^- and CrO_4^{2-} (figures 2 and 1 (curve b)), this is clearly resolved at both the L_3 and L_2 edges, while for the other oxyanions this splitting is smaller in magnitude and appears only as a low-energy shoulder on the considerably broader L_2 edge. Furthermore, close inspection reveals the presence of a weak feature W prior to the

Table 2. Absolute energies (and intensity ratios) of the various near-edge features at the O K edges of the transition-metal oxyanions shown in figure 3. The absolute energy values are accurate to ~ ±0.5 eV. Approximate intensity ratios were determined by a Gaussian fitting procedure. The data for $KMnO_4$ should be viewed with caution—see the text.

Oxyanion	Peak position (eV) A	Peak position (eV) B	Intensity ratio I_A/I_B
MnO_4^-	530.1	531.4	0.9
CrO_4^{2-}	529.8	531.2	0.6
VO_4^{3-}	530.2	531.5	0.5

main L_3 edge, which is most clearly seen in figures 1 (curves b–d) and 2. Additional weak structure is also apparent prior to the L_2 edge; this is most obvious in the $PbCrO_4$ spectrum (figure 1 (curve b)) but also appears to be present in $Pb_5(VO_4)_3Cl$ (figure 1 (curve c))—we discuss the origin of this latter feature in section 4.3.

The splitting at the L_3 edge is also reflected as a splitting of the first main feature at the O K edge into two components, which we also denote as A and B. We discuss the reasons for this below.

The data for $PbCrO_4$ are in good agreement with the lower-resolution data of Kurata *et al* [10] on K_2CrO_4, which also contains the CrO_4^{2-} anion. They observed a splitting of 2.2 eV at the Cr L_3 edge and a splitting of 1.3 eV at the O K edge; however, their absolute energy scale is slightly higher than ours.

The general trends observed for the metal L_3 and O K edges of the isoelectronic series of oxyanions may be summarized as follows:

(i) The L_3/L_2 white-line intensity ratio decreases in the order $MnO_4^- > CrO_4^{2-} > VO_4^{3-} > TiO_4^{4-}$. Estimates of the L_3/L_2 ratios were obtained by approximate extrapolation and subtraction of the underlying continuum contribution; the results were 1.6, 1.5, 1.0 and 0.9 for MnO_4^-, CrO_4^{2-}, VO_4^{3-} and TiO_4^{4-} respectively. Clearly these values are not constant even though the formal d-electron count in these systems is zero. In addition, we also determined the sum of the intensities of the two white-line components normalized to the continuum contribution (this was taken to be a 10 eV wide window after the L_2 edge), as defined by Pearson *et al* [16]. This quantity varied in a similar fashion, decreasing along the series X=Mn–X=Ti in XO_4^{n-}. Finally, we compared the L_3/L_2 intensity ratios of both tetrahedrally and octahedrally coordinated Ti(IV) in the compounds Ba_2TiO_4 and $BaTiO_3$ (figures 1 (curve d) and 6 (curve c) respectively). The corresponding results were 0.9 and 0.6, the value for the octahedral case being significantly lower than that for the tetrahedral case. Clearly more work is required if accurate d-electron occupancies are to be extracted from ELNES spectra of transition-metal compounds. We attribute the observed variations to the significant effects of covalency in these materials; we discuss this point below.

(ii) The magnitude of the A–B splitting observed at the L_3 edge decreases in the order $MnO_4^- \simeq CrO_4^{2-} > VO_4^{3-} > TiO_4^{4-}$. The ratio I_A/I_B of the relative intensities of these two components also decreases in the order $MnO_4^- > CrO_4^{2-} > VO_4^{3-} > TiO_4^{4-}$. It is extremely difficult to determine the behaviour for MnO_4^- owing to the poor statistical quality of the spectrum. However, comparison with the XANES data seems to confirm these trends.

(iii) The magnitude of the A–B splitting observed at the O K edges decreases in the order $MnO_4^- \simeq CrO_4^{2-} > VO_4^{3-}$. The ratio I_A/I_B of the relative intensities of the two components, decreases in the order $MnO_4^- > CrO_4^{2-} > VO_4^{3-}$. The spectrum for MnO_4^- is seen to exhibit a much broader peak A than the other transition-metal oxyanions; such broadening hides the relatively large intensity of this feature (table 2).

4. Discussion

The site symmetries of the d^0 transition-metal ions in the compounds studied are all lower than perfect T_d. The average X–O bond lengths in the XO_4^{n-} oxyanions are 1.81 Å in orthorhombic Ba_2TiO_4 [17], 1.75 Å in $Pb_5(VO_4)_3Cl$ [18], 1.66 Å in $PbCrO_4$ [19] and 1.63 Å in $KMnO_4$ [20]. For simplicity, we shall assume, as a first approximation, that all of these represent perfect tetrahedral symmetry; we discuss the influence of distortions below. In order to analyse the observed $L_{2,3}$ ELNES, we initially begin with a brief discussion of the local unoccupied electronic structure in a transition-metal ion in T_d symmetry. We consider how this will be reflected in the atomic multiplet spectrum observed at the transition-metal $L_{2,3}$ edges and compare our results with the available calculations. We then discuss our findings within the chemically more intuitive framework of MO theory. This allows us to consider the effects of covalency and how this will affect the results and also govern the corresponding structure observed at the O K edges.

In perfect T_d symmetry, a simple point-charge model predicts that the crystal-field splitting of the metal d orbitals should be the reverse of the octahedral t_{2g}^*–e_g^* [7]. Thus the lowest unoccupied state is e^* (doubly degenerate) followed at higher energy by the t_2^* state (triply degenerate)—the subscript g is dropped since we no longer have inversion symmetry. Furthermore the magnitude of the tetrahedral splitting should be $\frac{4}{9}$ of that in octahedral symmetry provided that the metal–ligand distance does not change between the two environments. A schematic diagram of the splitting of the transition-metal d orbitals in the two environments is shown in figure 4. Thus for a d^0 transition-metal ion in T_d symmetry we have two available sets of vacant metal d orbitals. We would therefore initially expect to observe two peaks at both the metal L_3 and L_2 edges, with an intensity ratio of 2:3. However, we must also consider the effect of the 2p core hole produced during the excitation process and how this will affect the structure in the atomic multiplet spectrum.

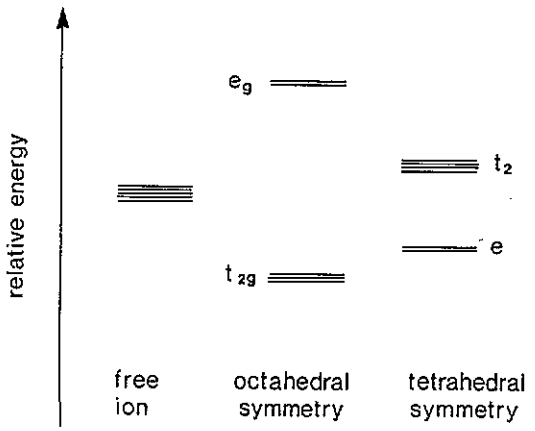

Figure 4. Schematic diagram of the splitting of the transition-metal d orbitals in octahedral and tetrahedral crystal fields.

4.1. Atomic multiplet theory

As stated in the introduction, although it is sometimes possible to identify crystal-field components, a proper analysis of the transition-metal $L_{2,3}$ spectra requires calculation of the

atomic multiplet structure in the presence of the tetrahedral crystal field. Such a calculation has been performed for Ti^{4+} (d^0) in T_d symmetry by both de Groot *et al* [5] (where the results are presented in terms of a negative crystal-field splitting) and van der Laan and Kirkman [9] for a variety of $10Dq$ values. Their calculations for a crystal-field splitting of between 1 and 1.5 eV looks most like our experimental spectrum for TiO_4^{4-} (figure 1 (curve d)). The calculations appear to reproduce the observed intensity ratio between the two components A and B at both the L_3 and L_2 edges. However, in order to achieve the correct intensity ratio, the magnitude of the splitting is slightly overestimated. The weak pre-edge feature W observed prior to the L_3 edge has been observed before in octahedrally coordinated transition-metal L_3 spectra [5, 6]. This weak pre-edge feature essentially arises from $p_{3/2} \rightarrow d_{3/2}$ transitions (strictly only in spherical symmetry) which are spin forbidden (i.e. they involve a change in spin) and are therefore of low intensity compared to the main L_3 components (A and B), which result from $p_{3/2} \rightarrow d_{5/2}$ transitions.

The atomic multiplet calculations also provide some explanation for the observed trend in the intensity rato I_A/I_B. From the results of van der Laan and Kirkman for Ti^{4+} [9] it is apparent that as the crystal field becomes weaker the ratio I_A/I_B becomes smaller and in the limit of zero crystal field the spectrum consists of two main lines plus a weak feature W. Assuming that we may apply the calculation for a transition-metal d^0 configuration (i.e. Ti^{4+}) to the other transition-metal ions, this would then explain the observed variation of I_A/I_B at the L_3 edge along the series $MnO_4^- - TiO_4^{4-}$. As the crystal-field parameter $10Dq$ decreases (this is reflected as a decrease in the separation between peaks A and B—see section 4.2), the ratio I_A/I_B would be expected to decrease as is experimentally observed. However, it should be also borne in mind that the I_A/I_B ratio will also change depending on the degree of lowered symmetry from perfect T_d.

It is not clear which final states give rise to the observed transitions in the calculated atomic multiplet spectra of Ti^{4+} in T_d symmetry. However van der Laan and Kirkman [9] make the point that for small crystal fields, the $2p^53d^1$ final states have mixed e^* and t_2^* character. As the strength of the crystal-field increases, the crystal-field components tend to become more apparent as individual spectral features. In section 4.2, we make the assumption that the two major features, peaks A and B, observed at both the transition metal L_3 and L_2 edges are predominantly associated with the crystal-field splitting of the transition-metal d orbitals. It could be argued that our subsequent analysis in terms of MO theory is somewhat questionable. Nevertheless we believe that the MO description does provide a degree of chemical insight that is absent from the atomic multiplet picture. Covalency effects are undoubtedly important in these transition-metal oxyanions, as is evidenced by the structure arising from O 2p–metal 3d hybridization (peaks A and B) at the corresponding O K edges. Covalency will essentially lead to a non-integer d count and a mixing of different final-state configurations, some of which will contain ligand holes [21]. This makes modelling using atomic multiplet theory considerably more complex and we therefore now consider the spectra in terms of MO theory, which should naturally include such covalency effects.

4.2. Molecular orbital theory

In order to provide a more quantitative version of crystal-field theory, the next step is to consider the MO structure of a d^0 XO_4^{n-} oxyanion as shown schematically in figure 5. There has been considerable debate concerning the relative ordering of the unoccupied MO energy levels, caused in part by a disagreement about the importance of π bonding in such oxyanions [22]. However, detailed consideration of optical data together with the results of more refined electronic-structure calculations appear to support the ordering scheme shown

in figure 5 [23]. The unoccupied MO structure consists of a doubly degenerate e^* MO separated by the crystal-field splitting from a triply degenerate t_2^* MO. In the case of solely σ bonding in XO_4^{n-}, the unoccupied e MO is formed solely from the d_{z^2} and $d_{x^2-y^2}$ atomic orbitals of the metal and is non-bonding (i.e. e^n), while the t_2^* MO is formed from overlap of the d_{xy}, d_{yz} and d_{xz} metal orbitals with the O 2p orbitals. The presence of additional π bonding in such oxyanions results in the additional mixing in of a considerable O 2p contribution into the unoccupied e MO (which is then antibonding in character, i.e. e^*) as well as some metal 4p and O 2s character into the unoccupied t_2^* MO. Both these MOs are accessible from both the metal 2p level and the O 1s level under the dipole selection rule.

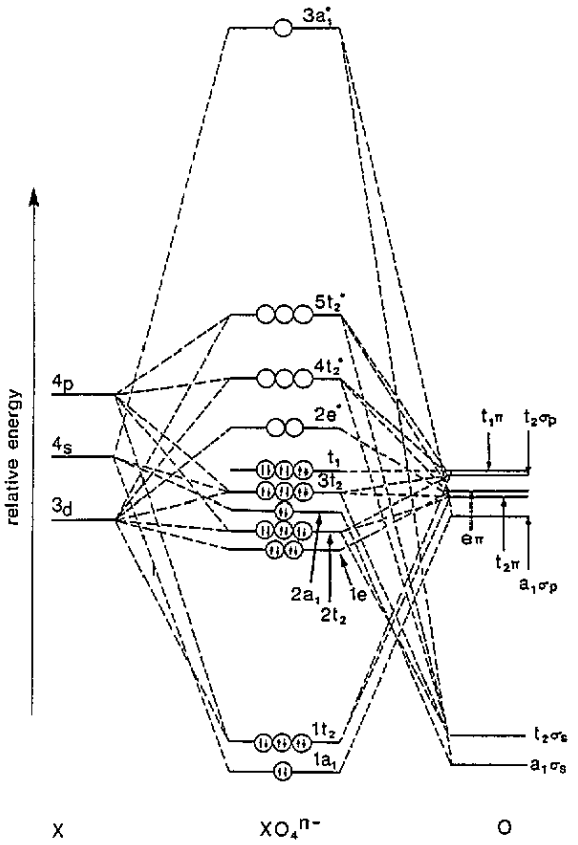

Figure 5. Proposed MO diagram for the XO_4^{n-} tetrahedral oxyanions (after [23]).

As a first approximation, we therefore propose that the observed splitting of the L_3 edge (and L_2 edge) into two components A and B is associated with transitions from the metal 2p level to the unoccupied e^* and t_2^* MOs of an XO_4^{n-} cluster, respectively. This splitting is also observed at the O K edges but is considerably different in magnitude. We now compare our observed splittings with those derived by both theory and experiment.

The magnitude of the ligand field splitting between the e^* and t_2^* antibonding MOs in the oxyanions may be obtained via consideration of the results of optical and UV spectroscopic measurements. Such spectra record the transition energies from the highest

occupied electronic energy levels to these lowest unoccupied levels. Unfortunately there exists considerable debate as to the correct assignment of the observed transitions. Muller and Diemann [24] identify the e^*–t_2^* splitting for MnO_4^-, CrO_4^{2-} and VO_4^{3-} as 1.2, 1.2 and 1.0 eV respectively. They also provide data for $TiCl_4$, which should be similar to TiO_4^{4-}, which gives an e^*–t_2^* splitting of 0.9 eV. Different assignments give larger e^*–t_2^* splittings, i.e. 1.6 eV in CrO_4^{2-} [25] and 1.7 eV in MnO_4^- [26].

A large number of theoretical calculations have been performed for the XO_4^{n-} oxyanions. These give a variety of results for the e^*–t_2^* separation, which often depends on whether a transition state (i.e. relaxation) procedure was used to model the optical excitation process. Inclusion of the latter effect generally reduces the e^*–t_2^* energy splitting. Gubanov *et al* [27] and Johnson [28] have used the multiple-scattering $X\alpha$ method to calculate the electronic structure of the XO_4^{n-} oxyanions (X=Mn, Cr and V). They found the e^*–t_2^* splittings to be 2.4, 2.1 and 1.6 eV for the MnO_4^-, CrO_4^{2-} and VO_4^{3-} oxyanions respectively. Bianconi *et al* [29] have performed similar calculations for the MnO_4^- and CrO_4^{2-} species, which gave splittings of 2.3 and 2.1 eV respectively. An almost identical calculation by Kutzler *et al* [30] gave a splitting of 2.0 eV for the CrO_4^{2-} anion. Various other calculations for the MnO_4^- ion are listed in the article by Nakai *et al* [31].

Despite the relatively large variation in both the theoretical and experimentally interpreted results, the general trend in the magnitude of the e^*–t_2^* splitting in the XO_4^{n-} oxyanions is found to be $MnO_4^- > CrO_4^{2-} > VO_4^{3-} > TiO_4^{4-}$. This fact is reflected in our observed A–B peak separations at the transition-metal L_3 and O K edges (tables 1 and 2) and is presumably due to the increase in the average X–O bond lengths and decreasing formal charge on the transition-metal ion that would be expected from the point-charge (crystal-field) model.

Our observed e^*–t_2^* splittings at the O K edges of MnO_4^-, CrO_4^{2-} and VO_4^{3-} are 1.3, 1.4 and 1.3 eV respectively. As observed by de Groot *et al* [8] for a variety of transition-metal oxides, the magnitude of the splitting at the ligand (O) edge agrees more closely with the ligand field splittings derived from optical measurements than the magnitude of the splitting at the transition-metal L_3 edge. The reasons for this are discussed in section 1. It should be noted that one problem in deriving ligand field splittings from the O K edges of these materials may lie in the presence of crystallographically inequivalent O sites within the unit cell. This will lead to differing O environments, which may lead to a superposition of differing O K ELNES and so complicate a simplistic analysis of the observed structure.

We may estimate the relative intensities of the two e^* and t_2^* components at both the metal $L_{2,3}$ edges and the O K edges of XO_4^{n-}. These intensities will be proportional to the metal- and O-derived contributions to both the e^* and t_2^* MOs and these contributions are related to the squares of the eigenvectors in the MO expansion in terms of a linear combination of atomic orbitals (LCAO). We have employed the Mulliken population-analysis calculations of Viste and Gray on MnO_4^- [32] and scaled the results by the degeneracies of the two unoccupied levels. The results suggest that at the Mn $L_{2,3}$ edge, the e^*/t_2^* intensity ratio should be of the order of 0.58, while at the corresponding O K edge this ratio is calculated to be 0.78. These extremely simple predictions correlate reasonably well with the differences in observed intensities at the two edges of MnO_4^- (see tables 1 and 2), so providing some corroboration for our simplistic MO assignments. We are not aware of any similar theoretical data for the other oxyanions, hence we have performed some simple SCF–LCAO calculations on these clusters using the GAUSSIAN 90 code of Frisch *et al* [33] and STO-3G basis sets, which gave very similar results. However, as a general rule the predicted e^*/t_2^* intensity at the metal $L_{2,3}$ edge is considerably higher than that observed experimentally. We believe that the strong intensity of the t_2^* component (relative to the

e* component) at the metal $L_{2,3}$ edges is principally due to the mixing in of a significant amount of metal 4p character that occurs in tetrahedral symmetry. This is immediately apparent from the non-zero eigenvectors of the metal 4p orbitals in the expression for the lowest unoccupied t_2^* level obtained from our SCF–LCAO MO calculations on these d^0 XO_4^{n-} clusters. p → p-like transitions are dipole allowed under tetrahedral symmetry, owing to the lack of inversion symmetry in the cluster [34], and we believe that this contributes to the relatively large t_2^* intensity at the $L_{2,3}$ edges. The difference in the relative magnitudes of the matrix elements for p → d-like and p → p-like transitions in tetrahedral coordination is unknown at the present time.

Since the lowest unoccupied e* MO is essentially a π antibonding orbital constructed from the metal 3d orbitals and the O 2p orbitals, whereas the lowest unoccupied t_2^* MO has both σ and π antibonding character, the e^*/t_2^* intensity ratio should provide an estimate of the relative amount of π bonding in the XO_4^{n-} oxyanion. We have noted that on going from MnO_4^- to VO_4^{3-}, the e^*/t_2^* intensity ratio at the O K edge decreases. This observation suggests that the oxygen-derived $2p\pi$ component of the lowest unoccupied e* MO is smaller for the V oxyanion than the Cr or Mn oxyanions. This is in accord with the traditional chemical view that the amount of π bonding (multiple bonding) decreases in the order $MnO_4^- > CrO_4^{2-} > VO_4^{3-} > TiO_4^{4-}$, which is reflected in the increase in the X–O bond length along this series [35].

However, if we consider the e^*/t_2^* intensity ratio at the transition-metal L_3 edge this also decreases in the order $MnO_4^- > CrO_4^{2-} > VO_4^{3-} > TiO_4^{4-}$. This suggests that the metal-derived contribution to the lowest unoccupied e* MO is decreasing on going from X=Mn to X=Ti in XO_4^{n-}. This is the opposite to what we would intuitively expect since, in the absence of π bonding, this orbital should be almost entirely of metal d character and essentially non-bonding. The metal d contribution to this orbital should therefore increase with decreasing π bonding. How do we resolve this apparent anomaly? We believe that the metal-derived contribution to the e* MO is in fact increasing; however, the observed e^*/t_2^* intensity ratio decreases because the t_2^* intensity increases proportionately more. We postulate that this is due to a greater mixing in of metal p- (predominantly metal 4p-) derived states into the t_2^* MO as we progress from X=Mn to X=Ti in the XO_4^{n-} oxyanion series. Support for this postulation is obtained from the results of our SCF–LCAO MO calculations on the oxyanions. For MnO_4^- the metal p contribution to the unoccupied t_2^* MO is approximately 28% of the total metal (p+d) contribution, whereas the corresponding figures for CrO_4^{2-}, VO_4^{3-} and TiO_4^{4-} are 32%, 44% and 61% respectively. Further evidence is apparent in the theoretical studies of Gubanov *et al* [27]. In their calculated MO structures for the series MnO_4^-, CrO_4^{2-} and VO_4^{3-}, not only do they predict a decrease in the e^*–t_2^* energy separation as the series is traversed, but they also predict that the difference in energy between the predominantly metal d-like t_2^* MO and the predominantly metal p-like t_2^* MO (both of which are hybridized with O 2p character, the latter lying at higher energies) decreases in a similar fashion. The fact that these two t_2^* MOs (one predominantly metal d-like and the other predominantly metal p-like) are becoming closer in energy suggests that an increase in metal d–p mixing (predominantly 3d–4p) is occurring. This would then suggest that the metal p contribution to the lowest t_2^* MO increases on going from MnO_4^- through CrO_4^{2-} to VO_4^{3-}.

Finally we consider the effect of distortions from perfect tetrahedral symmetry. This should primarily affect the t_2^* component at both the $L_{2,3}$ and O K edges since it is this component that is of σ antibonding character. Large distortions should lead to a splitting of this peak as is observed in the work of Jasinski *et al* [36, 37]. The distortions present in the materials studied in this work do not appear to lead to any observable splitting.

4.3. Multielectron excitations

So far we have accounted for the majority of the observed structure in terms of the atomic multiplet picture and subsequently restyled the discussion from the viewpoint of MO theory. The only remaining anomaly is the extremely weak structure observed prior to the L_2 edge, which cannot be accounted for by the atomic multiplet spectrum of a d^0 transition-metal ion in T_d symmetry [9]. Consideration of the work of Bianconi *et al* [29] on the K edges of these tetrahedral oxyanions leads us to the conclusion that this structure arises from a simultaneous two-electron excitation of both an inner 2p electron and of an electron in the valence band. These so called 'shake-up' satellites were also observed in the Cr 2p x-ray photoelectron spectrum (XPS) of K_2CrO_4, which also contains CrO_4^{2-} species, and their relative energy positions were theoretically predicted [29]. The intensities of these two-electron excitations are weak since the probability of such an occurrence is low. However, these multielectron excitations appear to be solely present in tetrahedral clusters [29], indicating that the component involving the excitation of a valence electron is a monopole (i.e. $\Delta l = 0$) transition.

4.4. Stability of tetrahedral oxyanions

A general point may be made concerning the relative stability of these tetrahedrally coordinated oxyanions. We have already mentioned the sensitivity of the MnO_4^- ion to electron-beam-induced damage and the subsequent transformation of Mn^{7+} to Mn^{4+} in the electron beam. However, $PbCrO_4$ also undergoes radiation damage. Intense electron-beam irradiation of this material resulted in a change in the Cr $L_{2,3}$ edge, from the spectrum shown in figure 1 (curve b) to one that more closely resembled Cr^{3+} in octahedral coordination [12, 10]. Furthermore, exposure of the Ba_2TiO_4 to the atmosphere resulted in the transformation of the Ti $L_{2,3}$ ELNES from the spectrum shown in figures 6 (curve a) and 1 (curve d), to that presented in figure 6 (curve b). The latter is characteristic of Ti^{4+} in octahedral coordination. The similarity of the ELNES of the transformed material (figure 6 (curve b)) to that observed in $BaTiO_3$, which contains octahedral TiO_6^{8-} groups and is shown in figure 6 (curve c), is striking. Indeed, the spectrum shown in figure 6 (curve b) appears to be a weighted sum of the spectra shown in figure 6 (curves a and c) suggesting that only part of the sample area under study had undergone transformation. From these results and the findings of previous studies [11], we propose that Ba_2TiO_4 transforms, in the presence of CO_2, to $BaTiO_3$ and $BaCO_3$. Thus, in consensus with established views, it appears that the relative stabilities of the tetrahedral oxyanions is not as great as those of the corresponding octahedral species.

The last observation has hinted at the possibility of using transition-metal $L_{2,3}$ ELNES as a probe of the local coordination symmetry around the transition-metal ion. This provides complementary information to the more established technique of valency determination using the white-line intensity ratios [2]. We believe that the relative intensities of the L_3 white-line components (i.e. in MO language the low e^*/t_2^* ratio) is characteristic of the tetrahedral d^0 oxyanions. Further studies of other tetrahedral and octahedral d^n transition-metal systems, such as those by Krishnan [38] and ourselves [12], are required for a more complete picture across the whole transition-metal period. Such a methodology represents an extension of previous K-edge XANES studies [29, 39, 40], where the presence of tetrahedrally coordinated-transition metal ions results in a characteristically intense pre-edge feature, which may be used for semi-quantitative analysis.

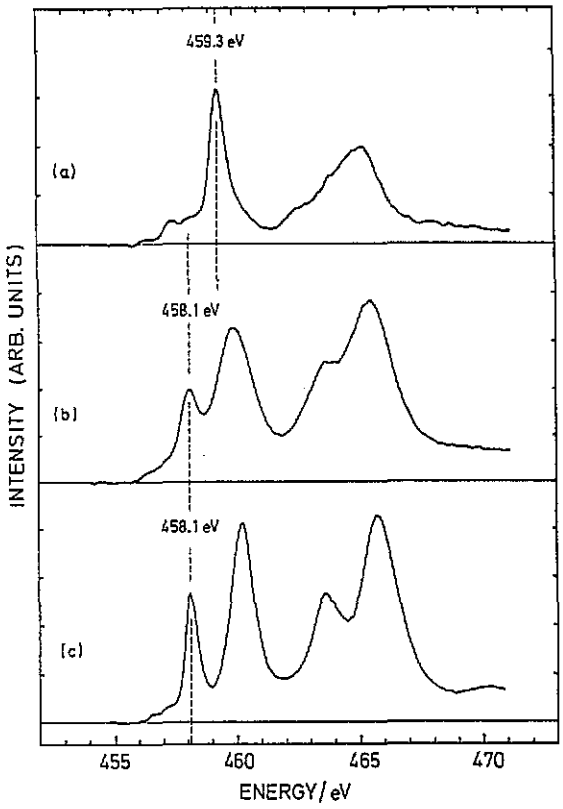

Figure 6. Ti $L_{2,3}$ ELNES of orthorhombic Ba_2TiO_4 (tetrahedrally coordinated Ti) (a), orthorhombic Ba_2TiO_4 after exposure to atmosphere (b) and $BaTiO_3$ (octahedrally coordinated Ti) (c). Spectrum b appears to be a weighted sum of spectra a and c. See the text for discussion.

5. Conclusions

We have presented the $L_{2,3}$ and O K edge spectra for a series of tetrahedral d^0 oxyanions XO_4^{n-}. The spectra show a remarkable similarity, especially at the L_3 edge, which we believe will allow them to be employed as coordination fingerprints. We have discussed the observed structures in terms of both atomic multiplet and MO theory and correlated the observed differences between the spectra in terms of variations in bonding and strength of the ligand field. It appears that the atomic multiplet picture more accurately describes the structure observed at the $L_{2,3}$ edge, while the MO picture is valid at the O K edge. However, in this work, we have demonstrated the utility of the MO description for the extraction of bonding information. It would be interesting to know the degree of overlap between the MO and atomic multiplet pictures for the case of the $L_{2,3}$ edges of tetrahedrally coordinated d^0 transition-metal ions where the final-state interactions are considerably less than for d^n species. Further work is required to clarify this point.

Acknowledgments

This work was originally initiated with financial support to one of the authors (RB) from the Royal Society. AJC would also like to thank the SERC for providing funds to purchase the

Gatan PEELS and for a research assistantship to one of us (LAJG). We also thank Professor E Zeitler for continued support.

References

[1] Brydson R 1991 *EMSA Bull.* **21** 57
[2] Brydson R, Sauer H and Engel W 1992 *Applications of Transmission Electron Energy Loss Spectrometry in Materials Science* ed M M Disko, C C Ahn and B Fultz (Warrendale, PA: TMS) p 131
[3] Waddington W G, Rez P, Grant I P and Humphreys C J 1986 *Phys. Rev.* B **34** 1467
[4] Thole B T and van der Laan G 1988 *Phys. Rev.* B **38** 3158
[5] de Groot F M F, Fuggle J C, Thole B T and Sawatzky G A 1990 *Phys. Rev.* B **41** 928
[6] de Groot F M F, Fuggle J C, Thole B T and Sawatzky G A 1990 *Phys. Rev.* B **42** 5459
[7] Figgis B N 1966 *Introduction to Ligand Fields* (New York: Wiley)
[8] de Groot F M F, Grioni M, Fuggle J C, Ghijsen J, Sawatzky G A and Petersen H 1989 *Phys. Rev.* B **40** 5715
[9] van der Laan G and Kirkman I W 1992 *J. Phys.: Condens. Matter* **4** 4189
[10] Kurata H, Ishizuka K and Kobayashi T 1988 *Bull. Inst. Chem. Res. Kyoto Univ.* **66** 572
[11] Marks M, Gunter J R and Hofer F 1988 *Reactivity Solids* **6** 217
[12] Garvie L A J, Craven A J and Brydson R 1993 *Am. Mineral.* at press
[13] Egerton R F 1986 *Electron Energy Loss Spectroscopy in the Electron Microscope* (New York: Plenum)
[14] Engel W, Sauer H, Brydson R, Williams B G, Zeitler E and Thomas J M 1988 *J. Chem. Soc. Faraday Trans.* I **84** 617
[15] Cressey G 1993 personal communication
[16] Pearson D H, Ahn C C and Fultz B 1993 *Phys. Rev.* B **47** 8471
[17] Gunter J R and Jameson G B 1984 *Acta Crystallogr.* C **40** 207
[18] Dai Y and Hughes J M 1989 *Can. Mineral.* **27** 189
[19] Effenberger H and Pertlik F 1986 *Z. Kristallogr.* **176** 75
[20] Palenik G J 1967 *Inorg. Chem.* **6** 503
[21] van der Laan G, Zaanen J, Sawatzky G A, Karnatak R and Esteva J M 1986 *Phys. Rev.* B **33** 4253
[22] Muller A, Diemann E and Jorgensen C K 1973 *Structure Bonding* **14** 23
[23] Ballhausen C J and Gray H B 1965 *Molecular Orbital Theory* (New York: Benjamin)
[24] Muller A and Diemann E 1971 *Chem. Phys. Lett.* **9** 369
[25] Johnson L W and McGlynn S P 1970 *Chem. Phys. Lett.* **7** 618
[26] Holt S L and Ballhausen C J 1967 *Theor. Chim. Acta* **7** 313
[27] Gubanov V A, Weber J and Connolly J W D 1975 *J. Chem. Phys.* **63** 1455
[28] Johnson K H 1973 *Advances in Quantum Chemistry* vol 7, ed P O Lowdin (New York: Academic) p 143
[29] Bianconi A, Garcia J, Benfatto M, Marcelli A, Natoli C R and Ruiz-Lopez M F 1991 *Phys. Rev.* B **43** 6885
[30] Kutzler F W, Natoli C R, Misemer D K, Doniach S and Hodgson K O 1980 *J. Chem. Phys.* **73** 3274
[31] Nakai H, Ohmori Y and Nakatsuji H 1991 *J. Chem. Phys.* **95** 8287
[32] Viste A and Gray H B 1964 *Inorg. Chem.* **3** 1113
[33] Frisch M J *et al* 1990 GAUSSIAN 90 revision I (Pittsburgh, PA: Gaussian)
[34] Hansen P L, Brydson R and McComb D W 1992 *Microsc. Microanal. Microstruct.* **3** 213
[35] Cotton F A and Wilkinson G 1980 *Advanced Inorganic Chemistry* (London: Interscience)
[36] Jasinski J P, Holt S L, Wood J H and Moskowitz J W 1975 *J. Chem. Phys.* **63** 1429
[37] Jasinski J P, Holt S L, Wood J H and Asprey L B 1975 *J. Chem. Phys.* **63** 757
[38] Krishnan K M 1990 *Ultramicroscopy* **32** 309
[39] Greegor R B, Lytle F W, Sandstrom D R, Wong J and Schultz P 1983 *J. Non-Cryst. Solids* **55** 27
[40] Wong J, Lytle F W, Messmer R P and Maylotte D H 1984 *Phys. Rev.* B **30** 5596